

NASA Technical Memorandum 85819

(NASA-TM-85819) DELAMINATION GROWTH
ANALYSIS IN QUASI-ISOTROPIC LAMINATES UNDER
LOADS SIMULATING LOW-VELOCITY IMPACT (NASA)
27 P HC A03/MF A01

N84-27833

CSCL 11D

Unclassified
G3/24 19659

DELAMINATION GROWTH ANALYSIS IN QUASI-ISOTROPIC LAMINATES
UNDER LOADS SIMULATING LOW-VELOCITY IMPACT

K. N. SHIVAKUMAR AND W. ELBER

DTIC QUALITY INSPECTED

JUNE 1984

DEPARTMENT OF DEFENSE
PLASTICS TECHNICAL EVALUATION CENTER
ARRADCOM, DOVER, M. J. 07801



National Aeronautics and
Space Administration

Langley Research Center
Hampton, Virginia 23665



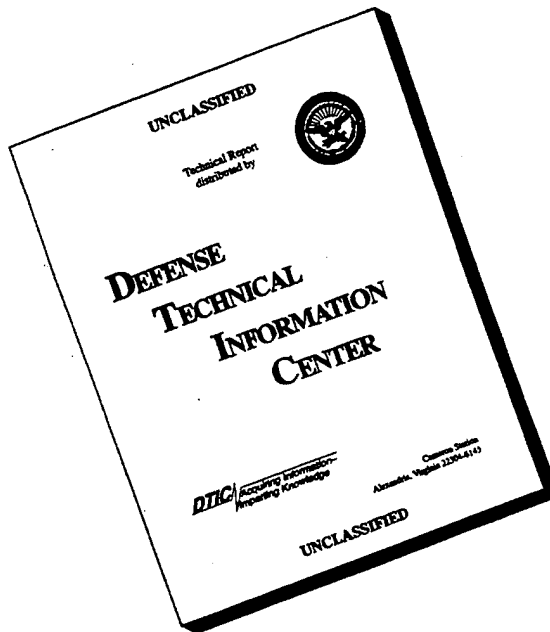
DISTRIBUTION STATEMENT A
Approved for public release;
Distribution Unlimited

19960312 116

44566



DISCLAIMER NOTICE



**THIS DOCUMENT IS BEST
QUALITY AVAILABLE. THE
COPY FURNISHED TO DTIC
CONTAINED A SIGNIFICANT
NUMBER OF PAGES WHICH DO
NOT REPRODUCE LEGIBLY.**

DELAMINATION GROWTH ANALYSIS IN QUASI-ISOTROPIC LAMINATES
UNDER LOADS SIMULATING LOW-VELOCITY IMPACT

K. N. Shivakumar* and W. Elber**
NASA Langley Research Center
Hampton, Virginia 23665

SUMMARY

A geometrically nonlinear finite-element analysis has been developed to calculate the strain energy released by delaminating plates during impact loading. Only the first mode of deformation, which is equivalent to static deflection, was treated. Both the impact loading and delamination in the plate were assumed to be axisymmetric. The strain energy release rate in peeling, G_I , and shear sliding, G_{II} , modes were calculated using the fracture mechanics crack closure technique. Energy release rates for various delamination sizes and locations and for various plate configurations and materials were compared. The analysis indicated that shear sliding (G_{II}) was the primary mode of delamination growth. The analysis also indicated that the midplane (maximum transverse shear stress plane) delamination was more critical and would grow first before any other delamination of the same size near the midplane region. The delamination growth rate was higher (neutrally stable) for a low toughness (brittle) matrix and slower (stable) for high toughness matrix. The energy release rate in the peeling mode, G_I , for a near-surface delamination can be as high as $0.5G_{II}$, and can contribute significantly to the delamination growth.

INTRODUCTION

Composite laminates made with high strength resin matrices are brittle and are easily damaged by transverse impact loads. Delamination damage

*Research Associate Professor, Old Dominion University.
**Senior Engineer.

commonly occurs under impacts by hard objects. Delaminations are usually invisible from the surface but still cause significant reduction in compressive residual strength of the laminate. The formation and growth of delaminations in laminated plates have recently been investigated under static loading (ref. 1). That study concluded that: (1) delaminations are formed in a laminate when the transverse shear around the contact area between the impactor and the plate exceeds a critical shear strength; (2) these delaminations grow if the shear strain energy release rate exceeds the matrix shear toughness. This report contains a finite-element formulation to predict the growth of an already created delamination in a circular quasi-isotropic laminate using fracture mechanics criteria. The model delaminations shown in figure 1 were used to assess the effects of delamination size and location on the strain energy release rate and delamination growth. Although backface damage is one of the common failure modes in thin plates under impacts, that problem is not addressed here. Instead, possible delaminations in thick plates are examined. For simplicity, the impact event is assumed to be equivalent to an axisymmetric plate loaded slowly in the direction of impact. This assumption is reasonable for quasi-isotropic plates impacted at the center.

Early studies at NASA Langley (refs. 2 and 3) of low velocity impact on 8 to 32-ply circular laminates have indicated that laminates may undergo large deflections, which makes the problem geometrically nonlinear. The objectives of this study are: (1) to develop a geometrically nonlinear axisymmetric finite-element (F-E) analysis which includes the crack closure technique of calculating strain energy release rates, (2) to identify the mode (opening or shear sliding) of delamination growth due to low velocity impact, (3) to examine the influence of delamination size and location and plate configuration on strain energy release rates, and (4) to examine the compression

instability of the near-surface delaminated layer due to impact. Figure 1 shows delamination models considered in this study. A midplane delamination (fig. 1(a)) was selected to identify the mode of delamination growth, i.e., mode I or II and/or combined. The critical location of the delamination was predicted by analyzing a plate with three delaminations; one at the midplane and the other two located at equal distances on each side of the midplane (see fig. 1(b)).

Compressive flexural stresses that develop during the impact of a thick laminate may cause local instability of delaminated surface plies. The local buckling of the surface sublamine results in high interlaminar peeling stresses in addition to shear stress at the delamination front. The mode of delamination growth therefore could be mode I, which is different from cases (a) and (b). To examine the energy release rates related to local instability, a plate with a delamination nearer to the top surface of the laminate, referred to as a near-surface delamination, was analyzed. Although more than one delamination may be present or created during the impact, for simplicity they are neglected.

A geometrically nonlinear two-dimensional finite-element program (ref. 4) was extended to include the axisymmetric case. The analysis includes calculation of strain energy release rates in the two possible fracture modes, namely the peeling (G_I) and the shear sliding (G_{II}) modes using the linear elastic fracture mechanics crack closure technique (ref. 5). Strain energy release rates for various delamination sizes and locations as well as plate configurations were calculated and compared.

SYMBOLS

a	plate radius, m
F	delamination front nodal force, N
G_I	strain energy release rate in peeling mode, J/m^2
G_{II}	strain energy release rate in shear sliding mode, J/m^2
G_{Ic}	fracture toughness in peeling mode, J/m^2
G_{IIC}	fracture toughness in shear sliding mode, J/m^2
h	plate thickness, m
P	static equivalent impact force, N
$q(r)$	contact pressure at r , N/m^2
$r-\theta-z$	plate cylindrical coordinate system
R_c	impact pressure distribution (contact) radius, m
R_δ	delamination radius, m
u	displacement in r -direction, m
w	displacement in z -direction, m
w_0	plate center deflection, m
z_δ	z -coordinate of a delamination, m
ΔR	element size around the crack tip

Subscripts:

$1,2$	nodes behind the delamination-front node
r,z	radial and z -directions

DESCRIPTION OF THE PROBLEM

Figure 2 shows a circular, quasi-isotropic laminated plate of radius a and thickness h , loaded by an elastic sphere at the center. The cylindrical coordinates for the plate are $r-\theta-z$. A section at $\theta = \text{constant}$ is shown in figure 2. The radial direction is r and the transverse direction is z . A midplane delamination of radius R_δ is shown in figure 2. The z -coordinate

of the delamination is represented by z_δ ; for midplane delamination $z_\delta = 0$. The impact by the sphere is assumed to be at the plate center and is represented by a static equivalent force P . The deformation of the quasi-isotropic circular laminate and sublaminates in the delaminated region are assumed to be axisymmetric. The radial and transverse displacements of the plate are represented by u and w , respectively. The contact force between the sphere and the plate is represented by an elliptical pressure distribution (ref. 6) (see fig. 3), such that $P = 2\pi \int_0^{R_c} q(r)r dr$, where $q(r)$ is the contact pressure at r . The radius R_c of the pressure distribution depends on the impact force and stiffness and curvature properties of the sphere and the plate (see, for example, ref. 7). For the range of forces and the sphere and plate considered here, the value of R_c varied from 0 to 1 mm. For simplicity, a nominal radius of 0.5 mm was assumed throughout the analysis.

ANALYSIS

A geometrically nonlinear, plane stress and plane strain finite-element (F-E) computer code GAMMAS (ref. 4) was extended to include axisymmetric analysis. The program uses a four noded isoparametric element. The methodology followed in the analysis is given in reference 8. A finite-element model for a midplane delamination is shown in figure 3. The linear elastic fracture mechanics (LEFM) crack closure technique (ref. 5) was employed to calculate strain energy release rates in mode I and mode II at the delamination front. A separate study was made to confirm the applicability of LEFM crack closure technique for calculating strain energy release rates in this geometrically nonlinear problem. Figure 4(b) shows a free-body diagram of the delamination front. Displacements in the r and z directions at nodes 1 and 2 behind the delamination front (node 0) are, respectively, u_1 , u_2 , w_1 ,

and w_2 (see fig. 4(b)). Delamination tip nodal forces in the r and z directions are F_r and F_z , respectively. Then, the strain energy release

rate in the peeling mode (I) is $G_I = \frac{F_z |w_2 - w_1|}{4\pi R_\delta \Delta R}$ and in the shear sliding

mode (II) is $G_{II} = \frac{F_r |u_2 - u_1|}{4\pi R_\delta \Delta R}$, in which R_δ is the delamination radius

and ΔR is the element size employed near the delamination tip. A fine F-E mesh ($\Delta R = 0.05$ mm or 0.1 mm) was employed around the delamination front.

Mesh refinement was studied to select a value of ΔR which yielded relative errors less than 1 percent. Strain energy release rates for various delamination sizes, locations, and plate configurations were calculated and the results are presented in the following section.

RESULTS AND DISCUSSION

Strain energy release rates in mode I and mode II for the typical delamination configurations shown in figure 1 were calculated using the linear elastic fracture mechanics crack closure criteria. The plate was assumed to be loaded statically by an equivalent impact force acting over a radius R_c (fig. 3). Energy release rates for various delamination sizes and location, and plate configurations and forces were calculated. Elastic material properties used in the analysis are given in table I. Results are discussed in the following sections.

A comparison of calculated G_I and G_{II} for the delamination configurations shown in figure 1 indicated that for delaminations away from the surfaces (figs. 1(a) and 1(b)) G_I is very small, less than 0.1 percent of G_{II} based on a deformed-configuration analysis. Hence, G_I results are presented only for near surface delaminations.

Midplane Delamination

Figure 5 shows the force P versus the plate center deflection w_0 for eight delamination radii (0 to 12.7 mm). As expected, the increase in delamination radius reduces the plate flexural stiffness, hence the initial slope of the force-deflection curve decreases.

Figure 6 shows the variation of G_{II} with force P for a range of delamination radii from 0.635 to 6.35 mm. An examination of the curves for various R_δ shows that for a constant force P , G_{II} decreases with an increase in delamination radius $R_\delta > 1.27$ mm. Therefore, the delamination growth stops after the initial growth. It is noted here that for R_δ less than or equal to $R_c + h/2$, the top compressive stresses reduce the effect of the shear stress singularity at the delamination front, with the result that calculated G_{II} values were small (see dashed curve $R_\delta = 0.635$ mm).

A method of predicting the delamination growth during loading is explained in figure 6. If a plate having mode II fracture toughness, say, $G_{IIC} = 1.0 \text{ kJ/m}^2$ and $R_\delta = 1.27$ ($R_\delta > R_c + h/2$) is loaded from zero by a steel sphere, the G_{II} increases from zero along the $R_\delta = 1.27$ curve (see fig. 6). At $P = 0.87 \text{ kN}$, G_{II} becomes equal to G_{IIC} (1.0 kJ/m^2). Further increase in the force P causes delamination to grow at constant $G_{II} = G_{IIC}$. The locus of G_{II} is shown by a broken line in figure 6. The plot of R_δ versus critical force P for a G_{IIC} of a laminate is hereafter referred to as "delamination growth curve."

Delamination growth curves for three materials whose elastic stiffness properties are the same as those for T300/5208 and with G_{IIC} values of 0.5, 1.0, and 1.5 kJ/m^2 are shown in figure 7. Each curve gives two values of R_δ for a selected force P . The smaller value corresponds to the case where the delamination lies within the impact pressure region and the larger value

ts for outside the region. For $R_S < R_c$, the compressive normal stress reduces the shear stress singularity at the delamination front, hence larger force is required for the delamination to become G_{II} critical. This force could exceed the material strength in transverse shear, tension, and/or crushing (see ref. 3). Therefore, the creation and initial growth of delaminations in and around the loaded region have to be governed by some other criteria like interlaminar strength criteria. The horizontal dash-dot line shown in the figure is the boundary ($R_S > 1.1$ mm) above which the present analysis (LEFM) is valid. Failure in the region below the broken line is controlled by interlaminar strength criteria. A large delamination $R_S > 1.27$ mm grows monotonically with the force. Furthermore, the rate of delamination growth (dR_S/dP) is greater for low values of G_{IIc} than for high values. Low values of G_{IIc} designate low toughness material.

The effect of impact force on energy release rate is shown in figure 8. Results for $R_S = 4$ mm and plate sizes 12.7×2 (radius \times thickness in millimeters), 12.7×3 , and 25.4×2 are shown. Calculated G_{II} decreased for both increased plate thickness (2 mm to 3 mm and radius 12.7 mm) and plate radius (12.7 mm to 25.4 mm) from the reference case (12.7×2). But, increasing thickness by 50 percent caused a much greater reduction in G_{II} than did doubling the plate's radius.

Figure 9 shows G_{II} versus force for T300/5208, C6000/HX205, C6000/F185, and T300/P1700 composites. Calculated G_{II} 's for all four materials are practically the same, even though their stiffnesses differ (see table 1). However, a delamination in a brittle composite (like T300/5200), which will have lower G_{IIc} , will become critical and grow at lower force than in tougher composites.

Multiple Delaminations

A laminate generally develops more than one delamination in thickness direction during the impact (see, for example, fig. 1(c)). A question is: which one of these delaminations is critical in the subsequent impact or transverse loading? To predict the location of a critical delamination, a plate with three delaminations was analyzed. One of the delaminations is at the midplane ($z_\delta = 0$) and among the remaining two, one is assumed to be above the midplane and the other below the midplane. Figure 10 shows strain energy release rate for three delaminations ($R_\delta = 4$ mm) located at $z_\delta = 0$ and ± 0.5 mm. The results indicate that G_{II} for the midplane delamination is higher than that for the other two. Therefore, a delamination in the midplane, which is a plane of maximum transverse shear stress, is most critical and grows before other delaminations in that region. It may be noted that the present analysis is based on homogeneous laminate properties. In an actual laminate, maximum shear stress location depends on the stacking sequence which is a function of layup and polar angle θ of the plate.

Figure 11 shows the predicted critical forces for initiation of growth of three delaminations. The material fracture toughness G_{IIC} is assumed to be 1.5 kJ/m^2 . For small delaminations ($R_\delta < 2.5$ mm) radii, the upper delamination (A) grows first followed by B and C delaminations. However, for $R_\delta > 3$ mm, the midplane delamination grows first and followed by A and C. These curves can be used to predict delamination radii for a given force by drawing an ordinate perpendicular to the abscissa as in figure 11. The intersection of the ordinate and the curves gives the delamination radii at the three locations. For example, an impact force of 2.5 kN causes delamination of radii 5.5, 4.4, and 4 mm at midplane, $z_\delta = -0.5$, and 0.5 mm, respectively.

Near-Surface Delamination

Compressive induced instability of delaminated laminas located near the impacted surface in a thick laminate was examined. If a thin debonded sub-laminate forms near the top surface of a laminated plate, it may buckle due to the compressive bending stresses developed by the transverse force on the plate (see fig. 1(c)). Large peel stresses caused by local buckling would tend to produce growth by mode I and mode II. Figure 12 shows energy release rates in both modes for delaminations located at $z_\delta = -0.75$ mm at a force $P = 2.4$ kN. The two curves indicate that, due to local buckling, the ratio of G_I to G_{II} could be as high as 0.5 ($R_\delta = 4$ mm). Since G_{Ic} of a material is much smaller than G_{IIC} , the delamination growth could be due to peeling alone. Both G_I and G_{II} decrease with increase in R_δ ($R_\delta > 4$ mm). Therefore, the delamination growth stops after an initial growth for a given force. For small values of R_δ ($R_\delta < 2$ mm) G_I decreases and G_{II} increases. Although more than one delamination can exist in a laminated plate, for simplicity and to narrow attention to compression buckling, only a near surface delamination was considered in the above analysis.

From figures 10 and 12 the values of G_{II} , for $P = 2.4$ kN and $R_\delta = 4$ mm, and for delaminations located at various values of z_δ are given below.

z_δ , mm	-0.75	-0.5	0.0	0.5
G_{II} , kJ/m^2	0.21	1.1	1.4	1.0

These results indicate that the delaminations near the midplane would have reached critical G_{II} and grown before a near-surface delamination becomes critical. The growth of near-surface delamination in mode II is, therefore,

less probable. However, the existence of G_I mode, even though small, can cause surface delamination growth since a material's G_{Ic} is far smaller than is G_{IIc} .

CONCLUSIONS

An axisymmetric finite-element analysis of a quasi-isotropic circular laminate under a static equivalent impact force led to the following conclusions:

1. The primary mode of delamination growth in the interior, away from top and bottom surfaces, of a circular, quasi-isotropic laminate subjected to transverse impact is by G_{II} (G_{III} was not addressed).
2. For a constant force, G_{II} decreases with increasing radius of the delamination when the delamination radius is greater than the loaded region.
3. Small delaminations (smaller than or nearly equal to the impact pressure area) have very low G_{II} 's due to a reduced shear stress singularity. Therefore, initial interlaminar failures may be governed by the interlaminar strength criteria.
4. Delamination growth rate is rapid (neutrally stable) for low fracture toughness (brittle) materials, and it is slow and stable for high toughness materials.
5. A midplane delamination, with a radius larger than the impact pressure radius, is more critical and grows faster than other delaminations of the same size but located in any other plane.
6. If a thin debonded sublamine forms near the impact surface of a thick laminate, the sublamine may buckle due to bending compressive stresses. The peel mode energy release rate G_I can be as high as $0.5G_{II}$. Therefore, a near-surface delamination in a material with low G_{Ic} may grow in the peeling mode.

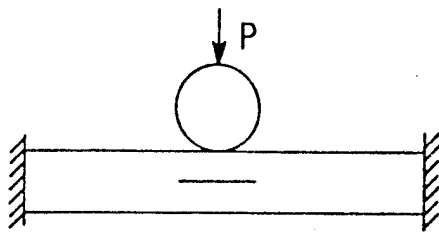
REFERENCES

1. Bostaph, G. M.; and Elber, W.: A Fracture Mechanics Analysis for Delamination Growth During Impact on Composite Plates. ASME Winter Annual Meeting, Boston, MA, Nov. 1983.
2. Elber, W.: Deformation and Failure Mechanics in Low Velocity Impacts on Thin Composite Laminates. NASA TP 2152, May 1983.
3. Shivakumar, K. N.; Elber, W.; and Illig, W.: Analysis of Progressive Damage in Thin Circular Laminates Due to Static-Equivalent Impact Loads. 24th AIAA/ASMB/ASCE/AHS, Structures, Structural Dynamics, and Materials Conference, Lake Tahoe, Nevada, May 2-4, 1983.
4. Whitcomb, J. D.; and Dattaguru, B.: Users Manual for GAMNAS - Geometric and Material Nonlinear Analysis of Structures. NASA TM 85734, Jan. 1984.
5. Rybicki, E. F.; and Kanninen, M. F.: A Finite-Element Calculation of Stress Intensity Factors by a Modified Crack Closure Integral. Engineering Fracture Mechanics, Vol. 9, 1977, pp. 931-938.
6. Goldsmith: Impact. Edward Arnold Ltd., London, 1960.
7. Greszczuk, L. B.: Damage in Composite Materials Due to Low Velocity Impact. Impact Dynamics, Ed. L. A. Zukas, et al., John Wiley and Sons, New York, 1982.
8. Zienkiewicz, O. C.: The Finite Element Method. McGraw Hill, New York.

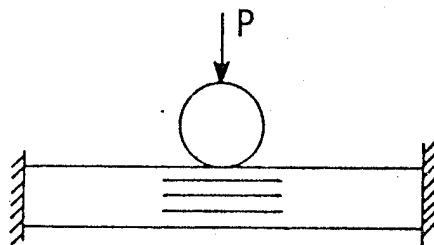
Table 1. Elastic properties of materials.

Parameter	Material			
	T300/5208	C6000/HX205	C6000/F185	T300/P1700
E_{rr} , GPa	54.00	48.33	44.35	37.56
E_{zz} , GPa	14.30	9.17	6.79	6.64
G_{rz} , GPa	3.50	4.10	2.70	2.62
v_{rz}	0.28	0.27	0.27	0.38
v_{r0}	0.31	0.31	0.32	0.32

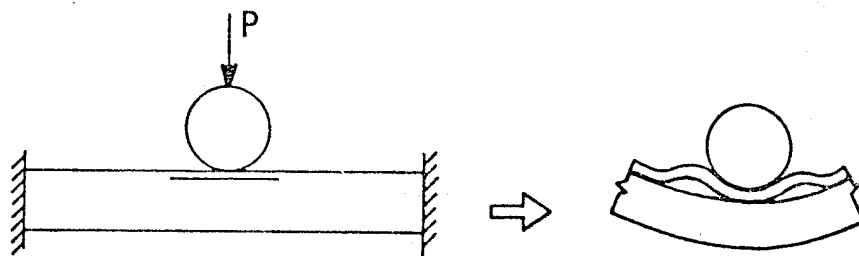
ORIGINAL PAGE IS
OF POOR QUALITY



(a) Mid-plane delamination.



(b) Multiple delamination.



(c) Near-surface delamination.

Fig. 1 Model delaminations.

ORIGINAL PAGE IS
OF POOR QUALITY

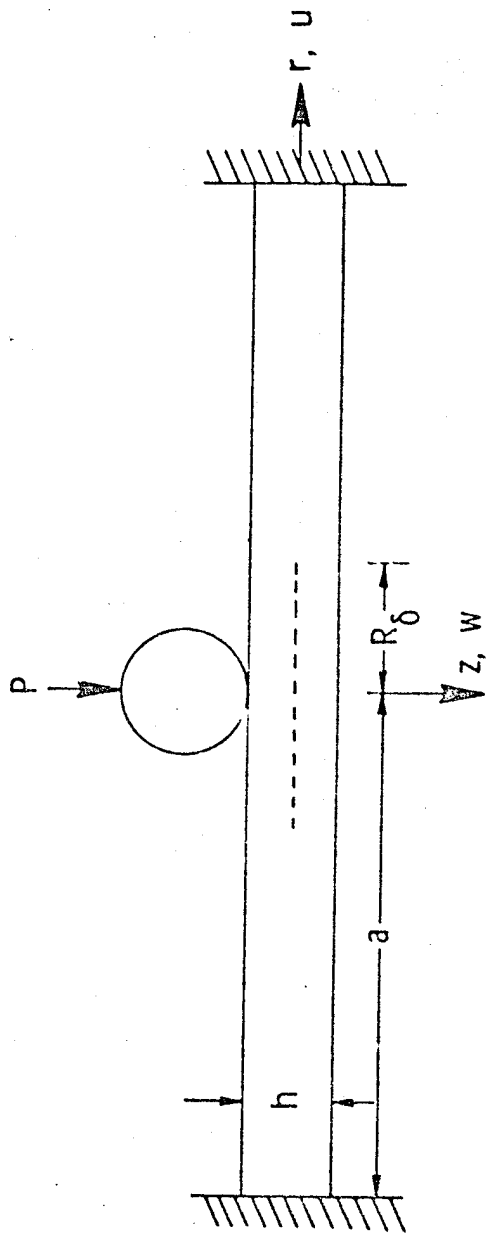


Fig. 2 Circular delaminated plate of radius a loaded centrally by an elastic sphere.

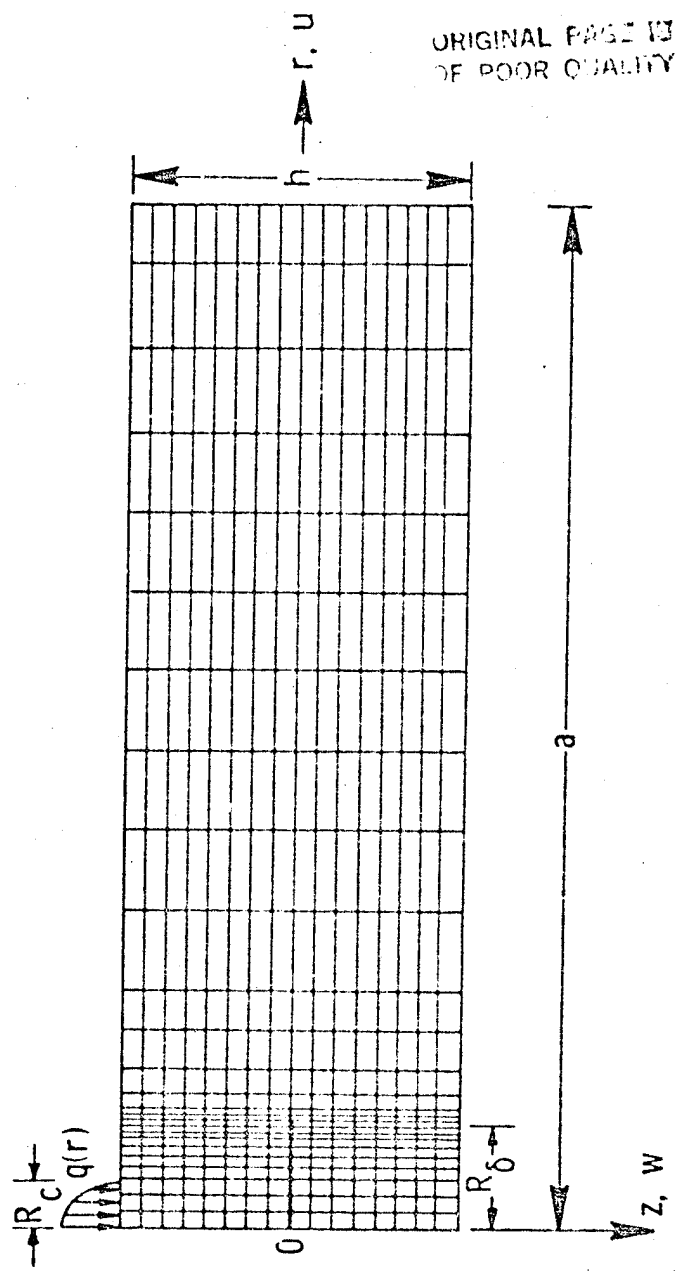
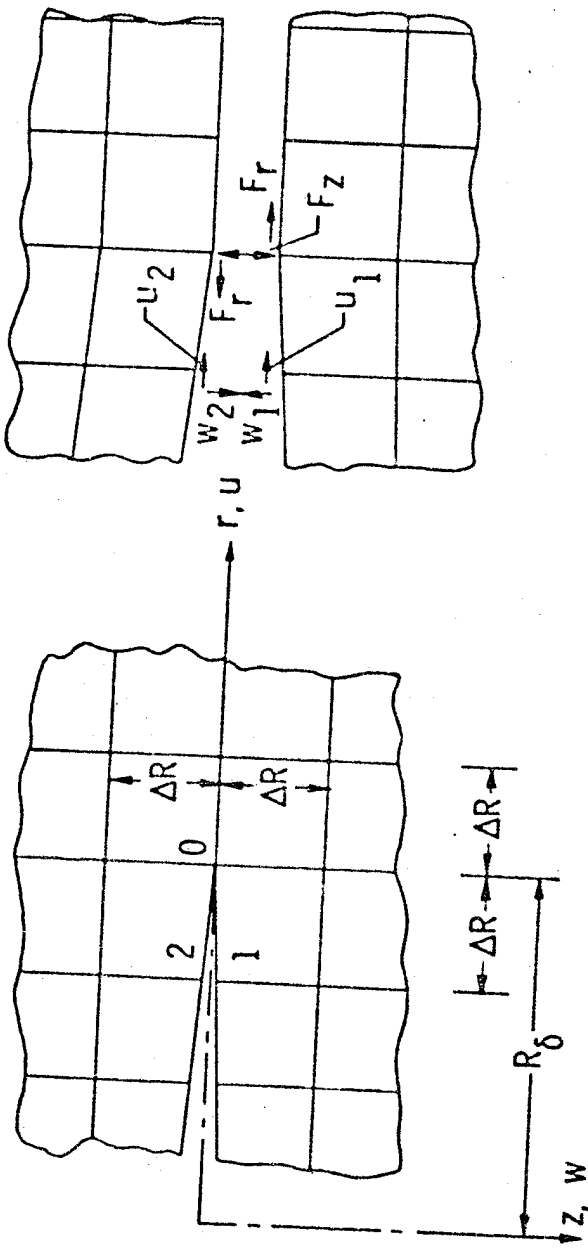


Fig. 3 Axisymmetric finite-element idealization of a mid-plane delaminated plate.



(a) Finite-element mesh around
the delamination front.

(b) Free-body diagram at the
delamination front.

Fig. 4 Nomenclature in the region of delamination front

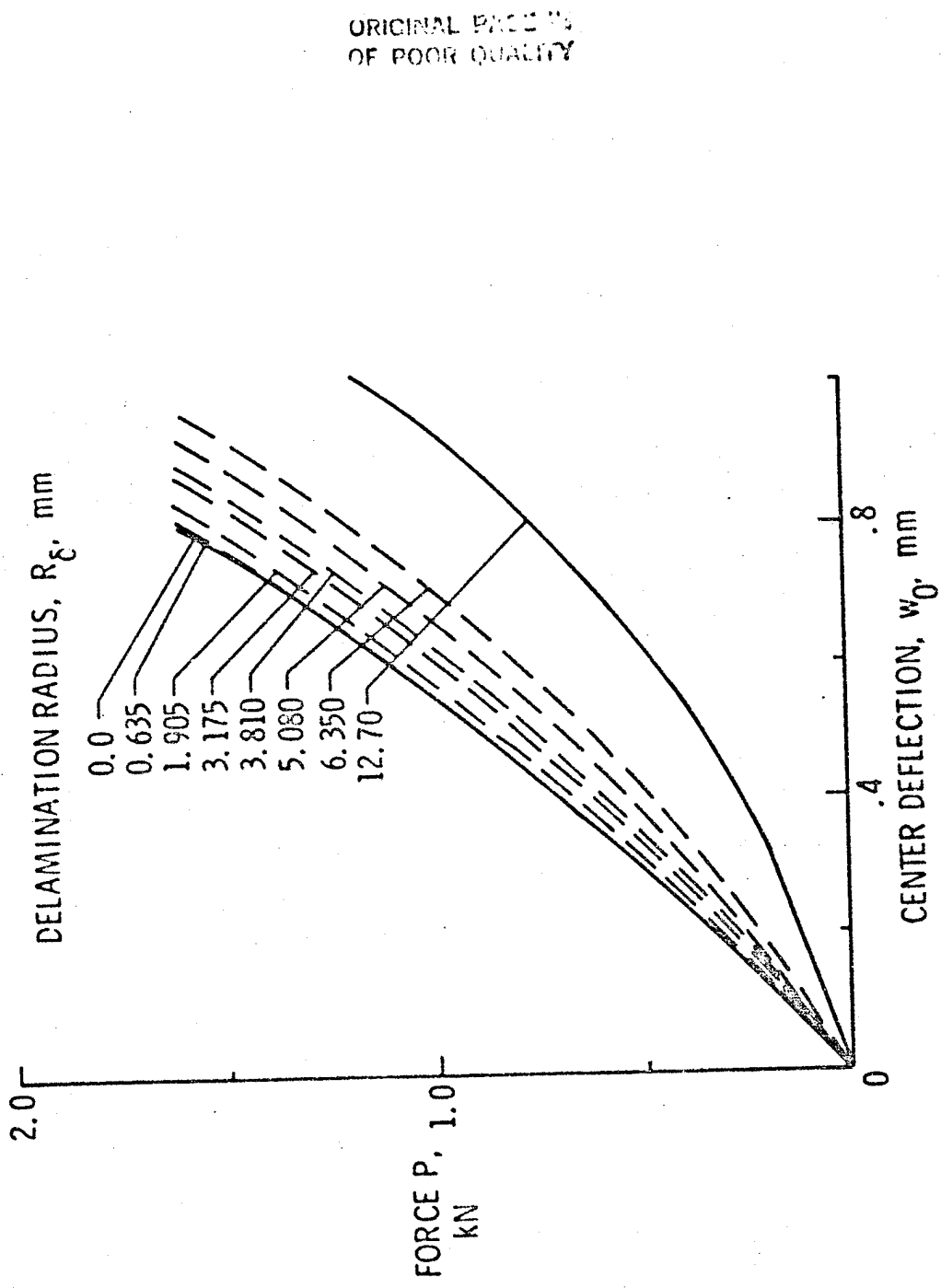


FIG. 5 Impact force versus deflection for a quasi-isotropic, circular plate
($a = 12.7$ mm, $h = 1.0$ mm, T300/5208)

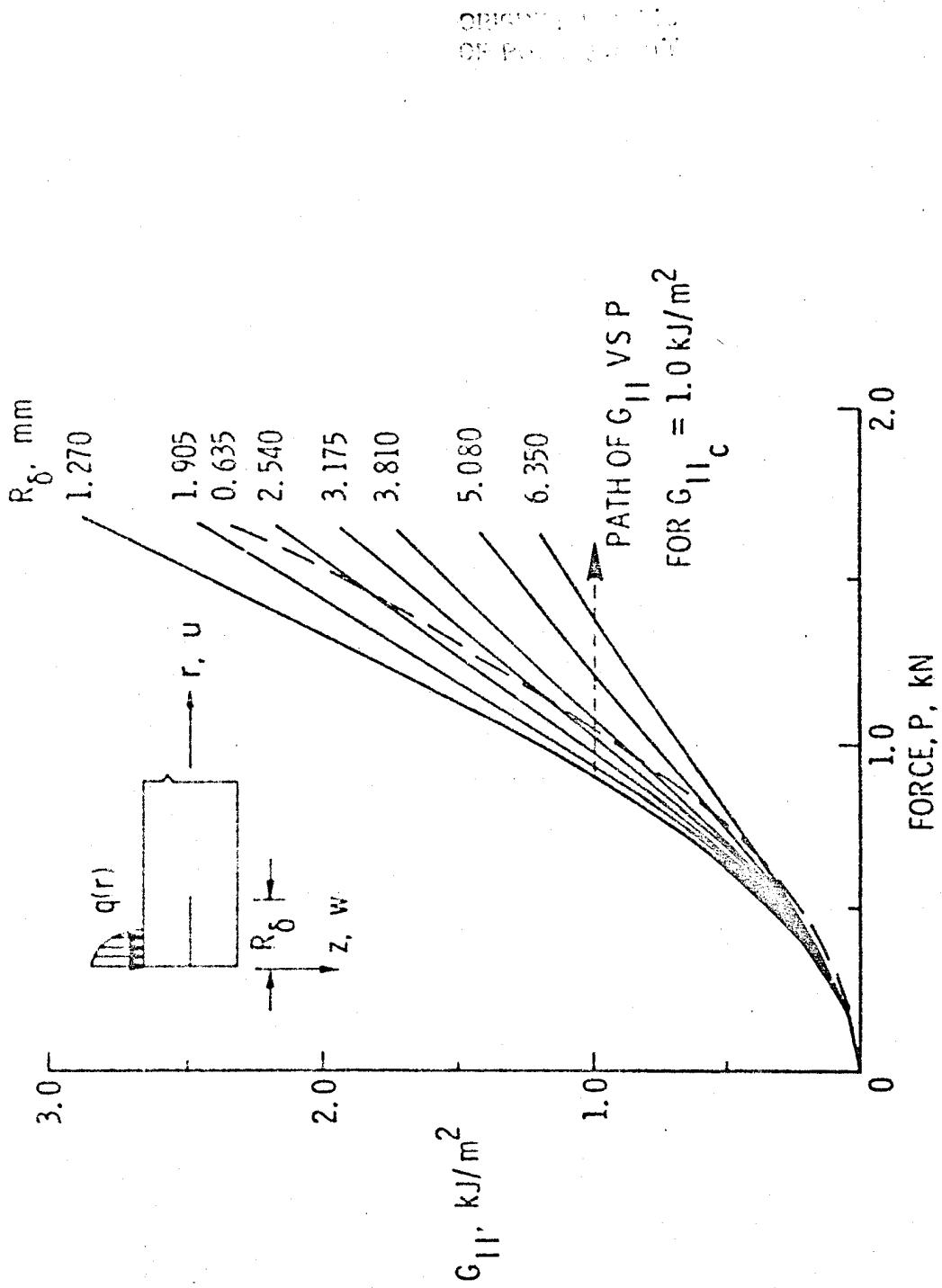


Fig. 6 Strain-energy-release rate G_{11} for various delamination radii.
 $(a = 12.7 \text{ mm}, h = 1.0 \text{ mm}, T_{300}/S208)$

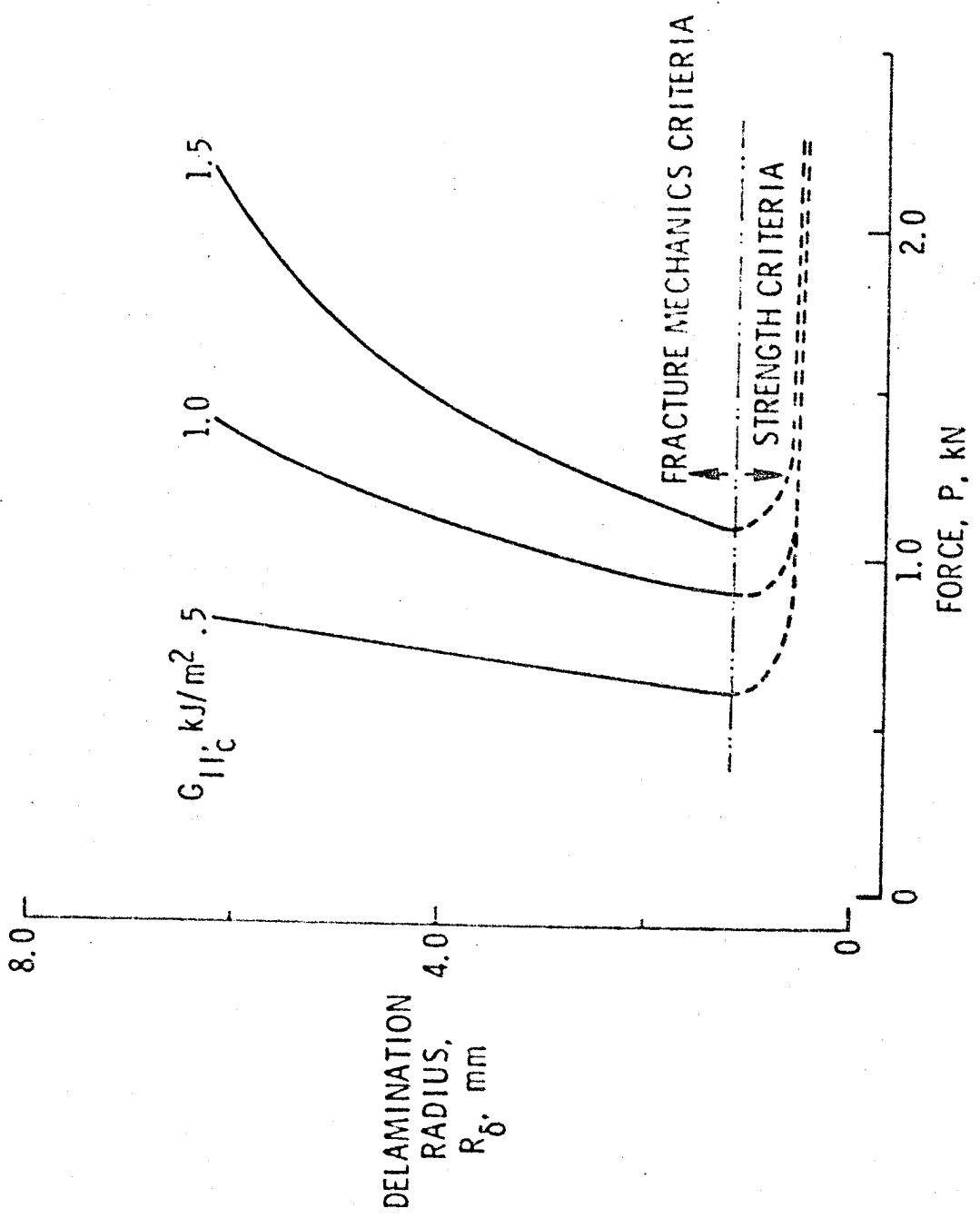


Fig. 7 Critical force versus delamination radius for various values of G_{IIc} .
 $(a = 12.7 \text{ mm}, h = 1.0 \text{ mm}, T300/5208)$

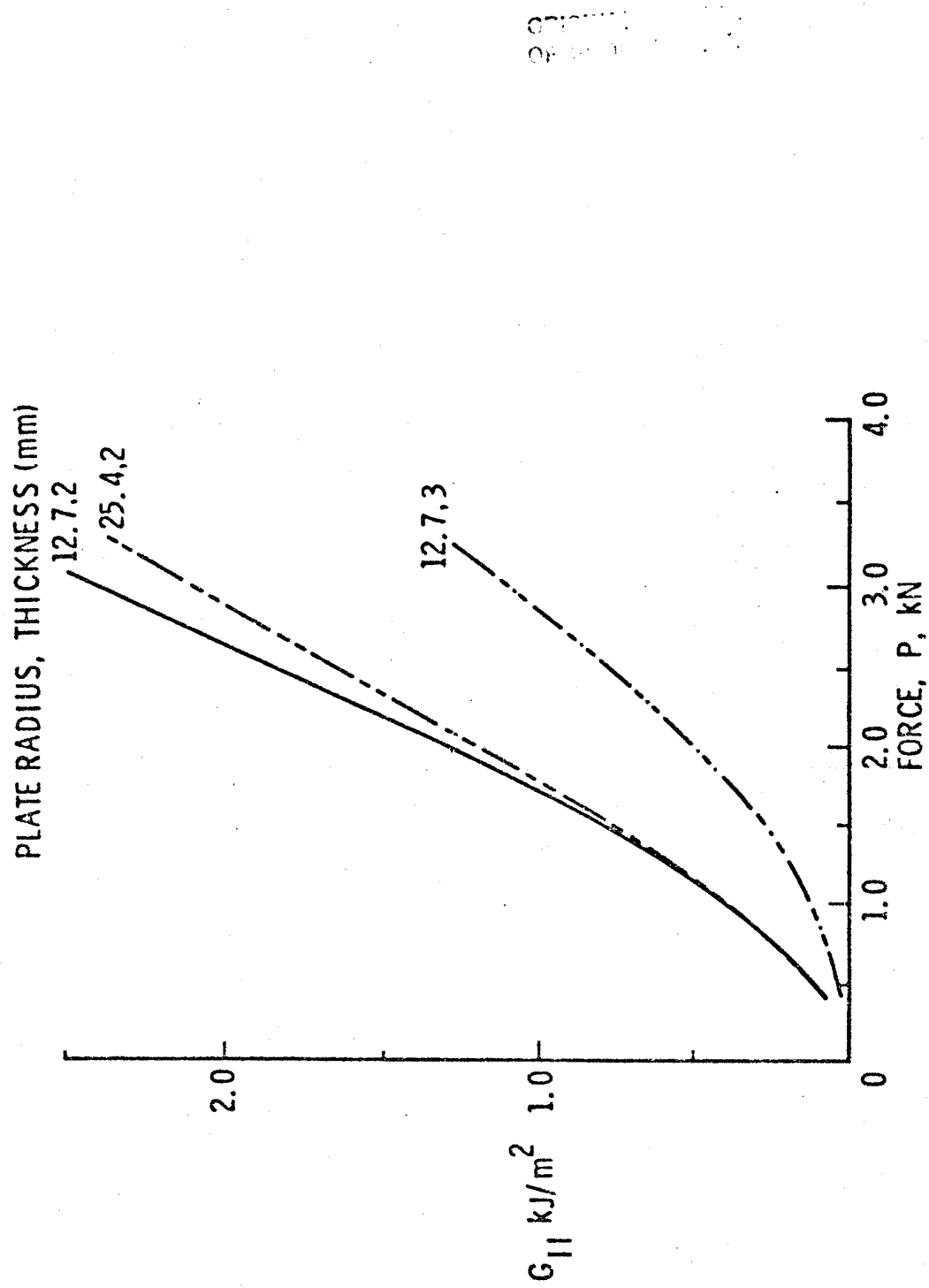


Fig. 8 Effect of force on G_{11} for three plate configurations.
 $(R_\delta = 4$ mm, mid-plane delamination, T300/S208)

ORIGINAL PAGE IS
OF POOR QUALITY

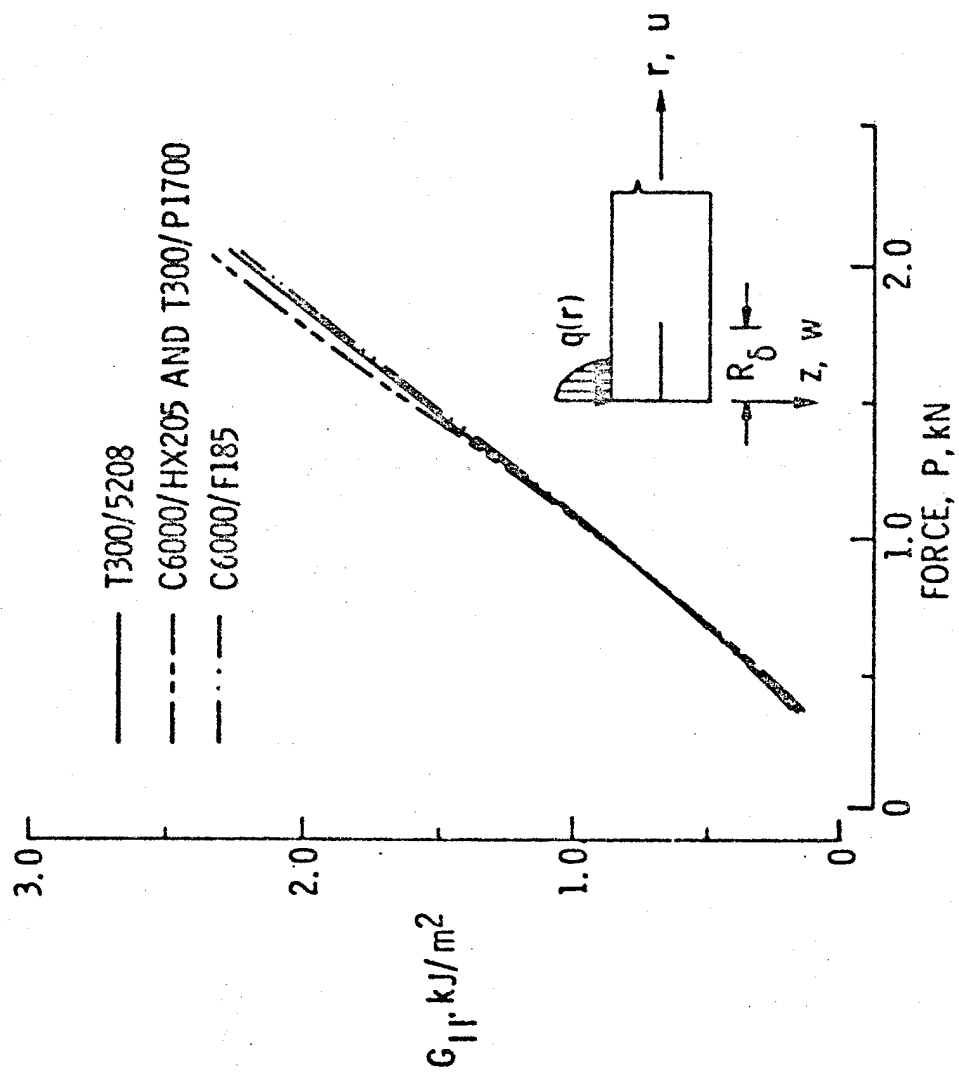


Fig. 9 Effect of force on G_{11} for various materials for a mid-plane delamination plate.
($a = 12.7$ mm, $h = 1.0$ mm, $R_d = 3.8$ mm)

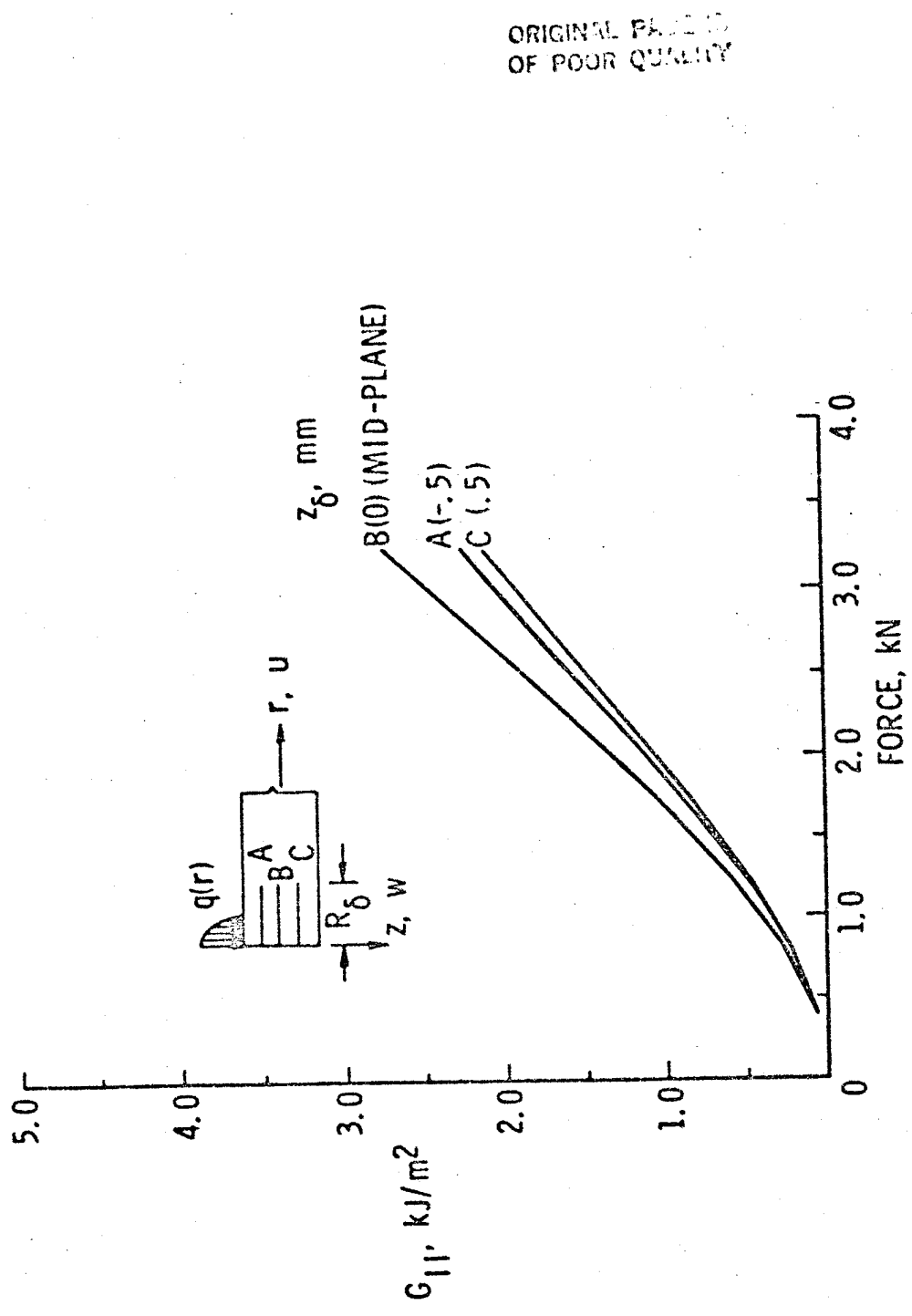


Fig. 10 Strain energy release rates for three delamination locations.
 $(a = 12.7 \text{ mm}, h = 2.0 \text{ mm}, R_\delta = 4.0 \text{ mm}, T300/5208)$

ORIGINAL PAGE IS
OF POOR QUALITY

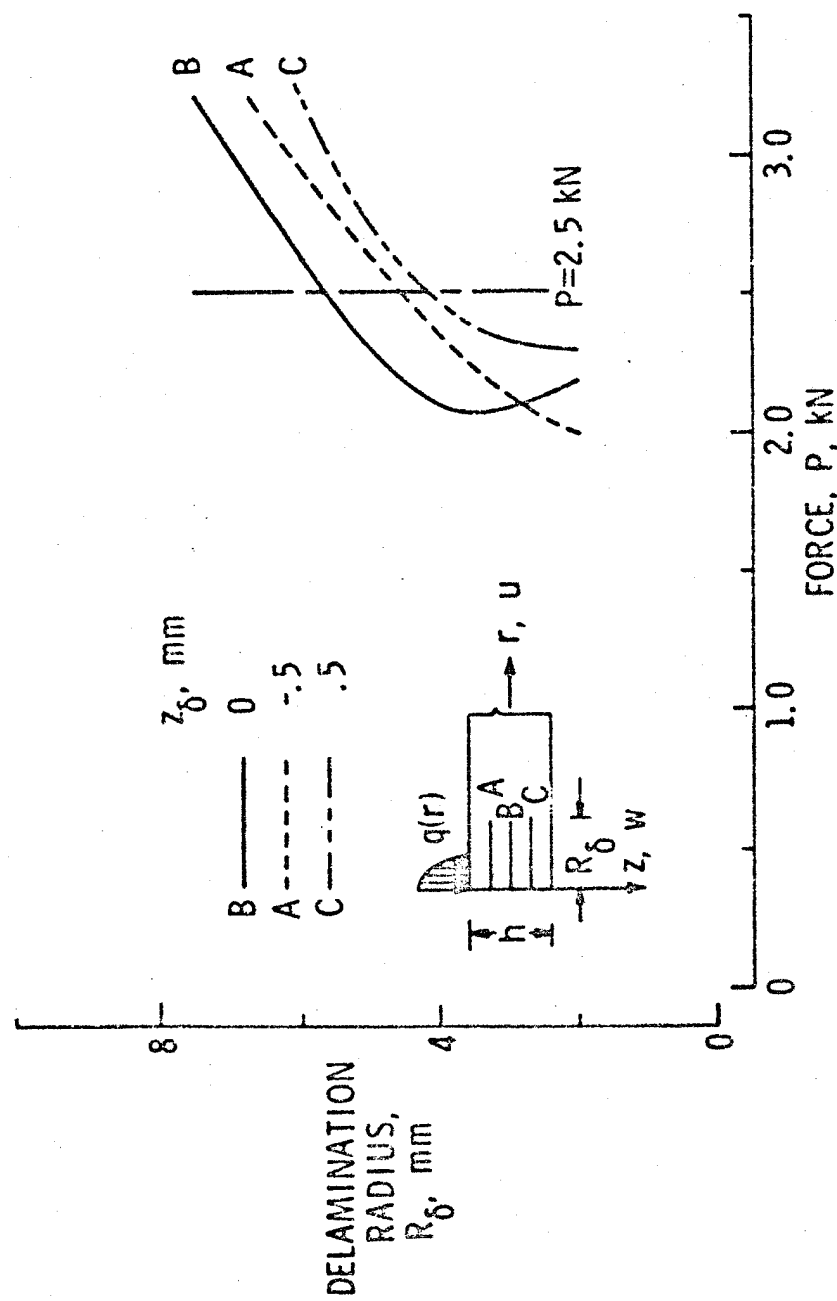


Fig. 11 Effect of force on radius of delamination for multiple delaminations.
 $(a = 12.7 \text{ mm}, h = 2.0 \text{ mm}, G_{llc} = 1.5 \text{ kJ/m}^2, T300/5208)$

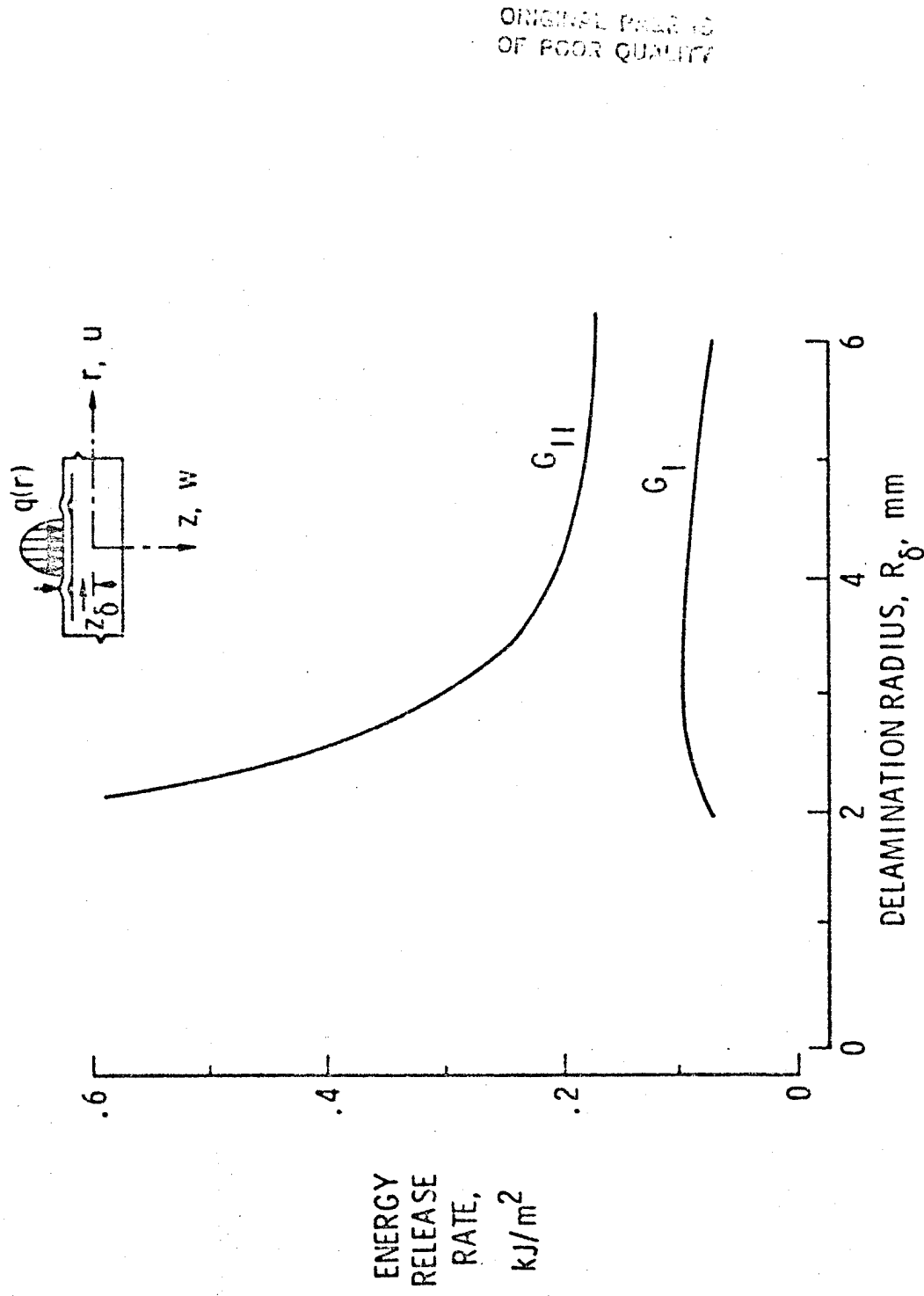


Fig. 12 Strain energy release rates for near-surface delaminations for $P = 2.4 \text{ kN}$.
 $(a = 12.7 \text{ mm}, h = 2 \text{ mm}, z_0 = 0.75 \text{ mm}, T300/5208)$